HHS Public Access

Author manuscript

Neuroimage. Author manuscript; available in PMC 2017 February 01.

Published in final edited form as:

Neuroimage. 2016 February 1; 126: 60–71. doi:10.1016/j.neuroimage.2015.11.022.

Real-Time Measurement and Correction of Both B0 Changes and Subject Motion in Diffusion Tensor Imaging Using a Double Volumetric Navigated (DvNav) Sequence

A. Alhamud[1,*], **Paul A. Taylor**[1,2], **A.J.W. van der Kouwe**[3,4], and **E. M. Meintjes**[1]

[1]MRC/UCT Medical Imaging Research Unit, Department of Human Biology, University of Cape Town, South Africa

[2]African Institute for Mathematical Sciences (AIMS), South Africa

[3]Athinoula A. Martinos Center for Biomedical Imaging, Massachusetts General Hospital, Charlestown, MA, USA

[4]Department of Radiology, Harvard Medical School, Brookline, MA, USA

Abstract

Diffusion tensor imaging (DTI) requires a set of diffusion weighted measurements in order to acquire enough information to characterize local structure. The MRI scanner automatically performs a shimming process by acquiring a field map before the start of a DTI scan. Changes in B0, which can occur throughout the DTI acquisition due to several factors (including heating of the iron shim coils or subject motion), cause significant signal distortions that result in warped diffusion tensor (DT) parameter estimates.

In this work we introduce a novel technique to simultaneously measure, report and correct in real time subject motion and changes in B0 field homogeneity, both in and through the imaging plane. This is achieved using double volumetric navigators (DvNav), i.e. a pair of 3D EPI acquisitions, interleaved with the DTI pulse sequence. Changes in the B0 field are evaluated in terms of zero-order (frequency) and first-order (linear gradients) shim. The ability of the DvNav to accurately estimate the shim parameters was first validated in a water phantom. Two healthy subjects were scanned both in the presence and absence of motion using standard, motion corrected (single navigator, vNav), and DvNav DTI sequences. The difference in performance between the proposed 3D EPI field maps and the standard 3D gradient echo field maps of the MRI scanner was also evaluated in a phantom and two healthy subjects. The DvNav sequence was shown to accurately measure and correct changes in B0 following manual adjustments of the scanner's central frequency and the linear shim gradients. Compared to other methods, the DvNav produced DTI results that showed greater spatial overlap with anatomical references, particularly in scans with subject motion. This is largely due to the ability of the DvNav system to correct shim changes and subject motion between each volume acquisition, thus reducing shear distortion.

[*]Corresponding author. Tel: +27 21 406 6128, Fax: +27 448 7226, alkk1973@gmail.com.

Keywords

diffusion tensor imaging (DTI); zero-order shim (frequency); the first-order shim (linear gradients); navigated diffusion sequence (vNav); double volumetric navigators (DvNav); B0 correction

Introduction

Diffusion tensor imaging (DTI) is widely used both clinically and in research. Applications of DTI include studies of brain maturation (Hasan et al., 2011; Miller et al., 2003; Mukherjee et al., 2001; Qiu et al., 2008; Schmithorst et al., 2002; Snook et al., 2005), white matter (WM) disorders (Engelbrecht et al., 2002; Noriuchi et al., 2010; Pavuluri et al., 2009), and functional and structural connectivity (Behrens et al., 2003; Bennett and Rypma, 2013; Itahashi et al., 2015; Staempfli et al., 2008).

Since the introduction of DTI (Basser et al., 1994), a large number of studies have investigated the presence, detection and reduction of artefacts in the data that can seriously affect results (Le Bihan et al., 2006). In addition to subject motion, magnetic field susceptibility artefacts and induced eddy current distortions are prevalent due to the fact that most diffusion weighted imaging (DWI) data are acquired using a combination of echo planar imaging (EPI) and strong magnetic field gradients. Some of these, such as eddy current distortions and subject motion, have been well-studied and both prospective and retrospective solutions have been proposed (Aksoy et al., 2011; Alhamud et al., 2012; Benner et al., 2011; Kober et al., 2012; Rohde et al., 2004). In contrast, the effects of changes in the static magnetic field (ΔB0) caused by motion or other sources on DTI data remain largely unaddressed.

Several factors can modulate the B0 field throughout the DTI acquisition, including subject motion (Ward et al., 2002), breathing (Pfeuffer et al, 2002), poor initial shimming, heating of the shim iron and mechanical vibration (Foerster et al., 2005; Benner et al., 2006). EPI acquisitions are particularly sensitive to effects of ΔB0 because of their long sampling time (tens of ms). ΔB0 effects occur predominantly along the phase encoding direction. B0 inhomogeneity leads to varying degrees of intensity and nonlinear geometrical distortions in the resulting volumes, typically producing detrimental features in DTI data. For example, a recent study by (Irfanoglu et al., 2012) found that EPI distortions can severely warp DTI brain volumes and deform fiber trajectories leading to erroneous inferences about brain structure and connectivity. Nonetheless, numerous DTI studies continue to be published without explicit correction for B0 distortions, relying instead on the active shimming process of the MRI scanner to fine-tune the homogeneity of the static B0 field before the start of the DTI acquisition and not accounting for subsequent changes in B0 that may occur due to motion or other sources.

Previous methods for correcting ΔB0 effects in EPI

Several techniques have been proposed to correct ΔB0 effects in EPI, including the use of specific hardware and both prospective and retrospective methods. Examples of hardware

that can contribute to distortion reduction in EPI include multichannel receive arrays used with parallel imaging (PI) techniques (Bammer et al., 2002; Pruessmann et al., 1999. In PI, acquisition is accelerated by collecting from different coil elements a subset of k-space lines and inferring the missing lines from a coil sensitivity map or kernel. Distortions are reduced due to the increase in effective bandwidth per pixel in the phase encoding direction. Although significant reductions in distortion have been reported, the specific coil and parallel imaging capabilities are not yet widely available on all scanners. It has also been reported that some distortion remains around tissue-air interfaces (Huang et al., 2008).

Prospective ΔB0 correction can be achieved using the EPI sequence itself or with additional pulses. Since EPI acquires echoes in alternating readout gradient directions, phase shifts between odd and even echoes occur and result in N/2 ghosting. Magnetic field inhomogeneity contributes to N/2 ghosting (Buonocore and Gao, 1997). Most commercial EPI sequences include a calibration scan to minimize N/2 ghosting. In this simple method, three non-phase-encoded k-space lines are acquired, two odd and one even, after slice excitation. Zero-order and linear phase errors are calculated and applied to the raw EPI data before Fourier transformation. A similar method, known as dynamic off-resonance in k-space (DORK) (Pfeuffer et al, 2002), was adapted to correct for respiratory induced off-resonance shifts in EPI. This uses the phase information from the navigator echo as well as from the imaging echo (self-navigator) at the center of k-space. Foerster et al. (2005) proposed a similar method to correct for drift in B0 by acquiring a simple one-dimensional free induction decay (1D-FID) immediately after each EPI acquisition in an fMRI sequence. The aforementioned methods can only correct drift in the B0 field that causes a shift in the imaging domain. They are unable to address geometrical distortion in EPI images that results from fluctuations in the linear and higher order terms of the B0 field. Additionally, the effectiveness of RF pulses, including fat saturation pulses, are reduced due to the drift in B0 and cannot be corrected with these methods (Benner et al., 2006). Subject motion may also affect the accuracy of these methods.

A more sophisticated method was proposed by Morell et al. (1997) and Lee et al. (2014) to correct in real time for the whole spectrum of B0 distortions, which includes zero- and first order shims. They appended a dual echo, multi-slice, gradient-recalled echo (GRE) sequence to the DWI-EPI sequence. For each slice, a field map is reconstructed on the fly, and zero- and first order shims are calculated. The field map acquisition time is about 1.6 s per slice. Two major disadvantages of this technique include the long acquisition time of the dual GRE sequence as well as subject motion during the acquisition of the field map or between DWIs.

Retrospective techniques for ΔB0 correction can be divided into three categories: B0 field maps, non-rigid image registration to a high resolution structural image, and the acquisition of additional EPI-DW images.

The field map method (Jezzard and Balaban, 1995) is a widely accepted approach in which B0 field inhomogeneity at every voxel is computed from phase images at different echo times that have been acquired with a gradient echo sequence before the start of the DTI scan. It has been reported that the correction is not entirely accurate in regions near edges with

high field inhomogeneity (Tao et al., 2009; Wu et al., 2008), for example where multiple voxels map singularly to one point. Moreover, its integration with parallel imaging poses further challenges (Huang et al., 2008).

The second category, which does not require a field map, is based on post-acquisition, non-rigid image registration techniques. In these approaches the EPI distortion of an acquired volume (e.g., a reference "b_0" image with b=0 s/mm^2) is co-registered to a high resolution, undistorted anatomical image, such as a T2- or T1-weighted (T1w) image, typically using a B-spline transformation (Kybic et al., 2000; Studholme et al., 2000; Tao et al., 2009; Wu et al., 2008). Wu et al. (2008) performed quantitative comparisons between this method and the field map technique. Their results showed that the standard field map-based methods tend to be superior in infratentorial regions, while deformable registration performs better in rostral brain regions. Since EPI images suffer from various artefacts that make image registration to structural images challenging, Irfanoglu et al. (2012) proposed a different way to estimate the amount of distortion. They compute the B0 field map from an initial segmentation of undistorted, T2-weighted structural images and tissue susceptibility models. The estimated B0 field map is then used to sample a non-uniform B-spline grid for an elastic registration-based correction step. Although non-rigid image registration approaches have shown some improvements for B0 inhomogeneity, they are nonetheless time consuming, remain virtually unused in routine DTI applications and also may have inherent performance limitations at higher gradient field strengths.

Others (Andersson et al., 2003; Holland et al., 2010; Ruthotto et al., 2012) have proposed using a combination of particular data acquisition and processing techniques. In this method two different sets of DTI acquisitions are acquired with different phase encoding directions, often termed "blip-up and blip-down", or "AP-PA" for their applied directionality (i.e., anterior-to-posterior, and vice versa). The ΔB0 correction is performed by calculating a deformation map between the two sets of b_0 reference volumes, which is then applied to all DWIs. This method can be implemented, for example, in FSL's topup program (Smith et al., 2004) or in TORTOISE (Pierpaoli et al., 2010), the latter of which also makes use of an anatomical reference. However, these approaches have the practical disadvantage of effectively doubling the scan time.

Dynamic shim fluctuations, including zero- and first order components that vary due to subject motion during the prolonged DWI-EPI acquisition, can substantially impact the effectiveness of retrospective correction methods or the inherent zero-order shim correction in EPI.

Proposed method for correcting ΔB0 effects: DvNav

In this study, we present a novel method to perform real time, volume-by-volume measurement and correction of B0 changes throughout the DTI acquisition, in terms of both frequency (zeroth order) and linear (first order) shim gradients. Furthermore, B0 correction is implemented while also performing simultaneous, real time motion correction using a fast, low resolution 3D EPI navigator, whose effectiveness has been demonstrated previously (Alhamud et al., 2012; Bhat et al., 2012; Hess et al., 2011; Tisdall et al., 2012). An additional, important feature of this corrective technique is that the accuracy of the ΔB0

estimate is not affected by the diffusion weightings themselves, and as such is effective even at high *b*-values such as are used in high angular resolution diffusion imaging (HARDI) (Tuch et al., 2002). Finally, the proposed method can also be broadly implemented, for example with functional MRI (fMRI) and in conjunction with parallel imaging technology and any radiofrequency (RF) coils.

Firstly, we demonstrate how efficient, low resolution ($8\times8\times8$ mm^3) double volumetric 3D EPI navigators (DvNav) with different echo times can be used to measure B0 changes in terms of zero- and first order shims throughout the DTI acquisition. Next, we evaluate the differences between the acquired 3D EPI phase map and the standard scanner 3D gradient echo phase map. We demonstrate that the DvNav can be used to measure and correct B0 changes in real time throughout the DTI acquisition. The method was validated both in the presence and absence of subject motion. Motion- and shim-corrected results are compared to those using only prospective motion correction (i.e., a single volumetric navigator) in order to demonstrate the added benefits of real-time B0 distortion correction.

Materials and Methods

vNav Sequence

The standard twice-refocused, 2D diffusion pulse sequence (Reese et al., 2003) was previously modified to perform prospective motion correction by acquiring one 3D EPI navigator (TR/TE = 14/6.6 ms, matrix 32 × 32 × 28) (Alhamud et al., 2012) in each TR. The volumetric navigator (vNav) contains low resolution ($8 \times 8 \times 8$ mm^3) 3D anatomical information for direct computation of motion parameters in real time. In the initial work by Alhamud et al. (2011), diffusion weightings of 700, 1400 and 2400 s/mm2 were applied, and it was observed that the navigator still provided reliable position estimates despite the possible effects of eddy currents induced by the large diffusion gradients in the navigator images. While long-term eddy current components may have subtle effects on the field map measured with DvNavs, such effects were not observed in the particular tests performed in the current study.

DvNav Sequence

In the current study, the diffusion sequence was further modified to acquire in each TR an additional 3D EPI navigator immediately following the first navigator with a different echo time (TE_1/TE_2 = 6.6/9 ms). This difference (ΔE = 2.4 ms) was chosen so fat and water are in phase at 3T. Using this double volumetric navigator (DvNav) approach one can correct simultaneously in real time both subject motion and $\Delta B0$. Motion correction is performed using the first of each pair of navigators in the “PACE” mechanism (Prospective Acquisition CorrEction; (Thesen et al., 2000)).

In the DvNav sequence, a field map is reconstructed for each DWI volume from the phase images of the two navigators. For accurate motion tracking, the navigator’s FOV has to cover the whole brain volume. To account for potential differences between the FOVs of the navigator and the DTI volume, the DTI’s FOV is mapped to the navigator’s field map to calculate the shim parameters over a smaller region. These calculations only take a few

milliseconds. This can be important if we are interested in shimming over a small FOV (or slice-by-slice) in DWI while using a larger field of view to track the motion of the entire brain, and we wish to minimize distortion separately for the two FOVs. Therefore, the zero order shim (ΔF, the shift in the scanner central frequency) and first order linear shim gradients (Gx, Gy and Gz) are calculated separately for the navigator and DWI volumes.

It is noteworthy that the DvNav sequence is independent of both the number and the ordering of the acquired reference b_0 (b=0 s/mm^2) and diffusion weighted (b>0 s/mm^2) volumes.

Sequence timing diagram for DvNav

Figure 1 shows the timing diagram of the DvNav sequence, in which subject motion and magnetic field inhomogeneity are measured and corrected. After the acquisition of the first navigator, the scanner reconstructs the magnitude and phase images. The latter are stored to be used later for the creation of the field map. Using the magnitude images, the subject motion parameters for the current acquisition are calculated and the results are initially stored without updating the scanner coordinates.

After acquiring the second navigator, the scanner creates a field map by way of complex division of the phase images. A whole head mask is also created from the magnitude image of the first navigator in order to exclude voxels with low signal-to-noise ratio (SNR). The intensity threshold utilized was a fifteenth of the mean signal intensity. This threshold was established empirically to optimize the exclusion of noise while not removing brain voxels. Field map phase unwrapping is performed online using PRELUDE (Jenkinson, 2003).

As a practical consideration, the FOV of the navigator is generally slightly different from that of the diffusion data. Volume adjustment is achieved by surrounding a cubic volume of interest (VOI) in the diffusion volume with six slice planes and then spatially mapping each plane to the navigator's field map. Although in theory the VOI may have any size, in this study it was chosen to enclose the entire DTI FOV.

Two pairs of frequency and first order shim estimates are calculated from each field map: one for the DTI VOI and one for the navigator FOV. Multiple linear regression, performed using a LAPACK routine (DGELS), is implemented to estimate shim parameters from both field maps. Before the start of the next diffusion volume, the DvNav sequence updates the DTI shim, and the slice coordinates and slice orientation to compensate for motion. After the next DWI volume has been acquired, the DvNav updates the shim for the next pair of navigators.

The shim updates are implemented as follows: The first order shim values are converted to currents. These values are then applied to the *x*-, *y*- and *z*- linear shim gradient coils. The correction for zeroth order shims (frequency offset) is achieved by recalculating the frequency and phase of all RF pulses and the phases of the acquired k-space lines. The total additional time added to the TR of each DWI is 1150 ms, which is comprised of the acquisition period for both navigators (2×475 ms); the period required for motion calculation, storage, and correction (80 ms); and time for shim calculation, storage and

correction (120 ms). Figure 2 is a flow diagram that summarizes how corrections for magnetic field inhomogeneity and subject motion are achieved simultaneously in the DvNav sequence.

It should be noted that shim correction is applied for the first time after acquisition of the first pair of navigators, which immediately follow the 1st DTI volume of the scan. Therefore, the correction for shim applies only to the 2nd DTI volume. We observed that shim correction of the human brain is not completely stable by the 2nd DTI volume, possibly due to motion-shim interactions, whereas in the water phantom scans the shim correction appeared to have completely stabilized after the 1st DTI volume. Since the pair of navigators that are used as reference volumes for motion correction should preferably be acquired after the shim has stabilized, simultaneous motion and shim correction only becomes fully effective after the 3rd set of navigators (i.e. at the start of the 4th DTI volume). Therefore, the first two acquired volumes should be considered as dummies, analogous to the common practice in fMRI where volumes acquired prior to attainment of the magnetization steady-state are discarded. As is often the case in the DTI sequence, the first acquired volumes in this study were reference b_0 images. Due to the shim stabilization, the total number of b_0's in this study was increased from 4 to 8 in both the DvNav and standard sequences to ensure that acquisition protocols were matched.

While the DvNav sequence calculates a 3D EPI phase map for ΔB0 correction, the default, scanner-produced field map on the Siemens Allegra is derived from a 3D gradient echo sequence with different echo times. From the field map the zeroth-, first- and second order shims are calculated and applied over the whole FOV of the diffusion data. In contrast to the the DvNav sequence, this is only done once at the start of the sequence for the standard sequence.

MRI Data Acquisition

Four healthy human subjects (27–35 years of age; male) and a water phantom were scanned using both the standard twice refocused spin echo EPI DTI sequence (Standard) (Reese et al., 2003) and the DvNav DTI sequence (DvNav). All scans were performed on an Allegra 3T scanner (Siemens Healthcare, Erlangen, Germany) using a single channel birdcage head coil in accordance with approved protocols. For each human subject, a T1-weighted (T1w) structural image was acquired using the motion navigated (Tisdall et al., 2012) multiecho magnetization-prepared, rapid gradient echo (MEMPR) sequence (van der Kouwe et al., 2008) with TR 2530 ms, TEs 1.53, 3.19, 4.86, 6.53 ms, TI 1100 ms, flip angle 7 deg, voxel size 1×1×1 mm^3 and matrix size 224×224×144. MEMPR was used in this study since it provides optimal contrast between gray matter and white matter, as well as CSF, with reduced B0 distortion due to the use of a higher bandwidth (van der Kouwe et al., 2008). In this study we assess the amount of EPI distortion during DTI acquisition with and without dynamic B0 shim correction by comparison with the relatively distortion-free MEMPR images.

The following parameters were used for each diffusion acquisition with the exception of the water phantom validation scans for frequency and linear gradient, where fewer slices and DWI volumes were acquired to reduce the degree of heating within the shim iron: TE 86 ms,

72 slices, in-plane matrix 112×112 and FOV 224×224 mm^2, slice thickness 2 mm, 30 non-collinear diffusion gradients with b=1000 s/mm^2 and eight b_0 scans. The TR values differed between acquisitions: TR=9500 ms for standard acquisitions, and TR=10650 ms for DvNav acquisitions (which includes the DvNav as well as all shim and motion calculations and adjustments). In the water phantom validation scans the same parameters were used, except that only 20 slices and the first 8 b_0 volumes were acquired (TR=3800 ms) in order to avoid a drift in the B0 field that was not related directly to the manual changes. For all scans, navigator parameters were: TR 16.2 ms, TE_1 6.6 ms, TE_2 9 ms, voxel size 8×8×8 mm^3, matrix size 32×32×28, FOV 256×256×224 mm^3, bandwidth 3906 Hz/px and flip angle 2 deg.

Scanning protocol and data analyses

(1) Validation of DvNav frequency and linear gradient measurements—A water phantom was first scanned using the DvNav DTI sequence to determine the accuracy of zero- and first order shim measurements.

Zero order shim (system central frequency) was assessed by performing 7 acquisitions, each comprising only eight b_0 volumes to prevent system frequency drift due to heating. After acquisition of a baseline scan with the initial system settings, the system frequency was offset for the remaining 6 acquisitions by 5, 10, 20, 40, 70 and 100 Hz, respectively. Since we wanted to determine the ability of the DvNav sequence to measure and correct effects of different magnitudes, a range of offsets were chosen based on values that had been reported previously. For example, Pfeuffer et al. (2002) reported that a single deep breath could change the dynamic off-resonance frequency by 2 to 8 Hz. Benner et al. (2006) observed that the frequency can drift by as much as 50 Hz during a single gradient-intensive DTI acquisition. El-Sharkawy et al. (2006), who performed experiments on different scanners with different types of MRI sequences, found that variations in the B0 field on a long time scale can result in frequency drifts of 100 to 300 Hz (0.8 to 2.5 ppm).

First order (linear) shim was validated using 4 acquisitions, each again comprising only eight b_0 volumes. After a baseline scan with the initial system shim settings, the shims were manually adjusted for the other 3 acquisitions by 15 μT/m in the *y*-direction, 15 μT/m simultaneously in *x*- and *y*- directions, and 15 μT/m simultaneously in *x*-, *y*- and *z*-directions.

For each of the above acquisitions, the changes in frequency (ΔF) and linear shim gradients estimated by the DvNav sequence were compared with known values from manual frequency and linear shim gradient adjustments. Color maps were also generated to visualise distortions/shifts arising from manual frequency adjustments, as well as the ability of the DvNav sequence to correct these distortions. We computed, in a representative slice, for each voxel the difference in normalised signal intensity between the second b0 image of a scan without an applied frequency shift (reference image) and the *first* b0 image of a scan with an applied frequency shift. The second volume of the reference scan was used since the shim would have been optimised after acquisition of the first navigator pair. Regions of greater distortion following the frequency adjustment will show higher signal intensity differences. To determine the extent to which the DvNav sequence is able to correct the

scanner frequency, and thus reduce distortions, prior to the acquisition of the second volume in the scan with an applied frequency shift, we also computed for each voxel the difference in normalised signal intensity between the second b0 image of a scan without an applied frequency shift (reference) and the *second* b0 image of a scan with an applied frequency shift. In each case, voxelwise differences were overlaid on the reference volume; the color scale represents the magnitude of the difference. In the same way, we visualised distortions arising from the applied linear shim gradient changes, as well as the extent to which the DvNav sequence could correct distortions arising from these gradient changes by adjusting the shim gradients.

Central frequency drift that may occur due to heating of the shim iron (Benner et al., 2006) or other sources within and between acquisitions was measured by performing five additional acquisitions (scans 1–5) on the water phantom without manual adjustment of either the scanner's linear shim or the system's central frequency. Each acquisition comprised 38 volumes (eight b_0 and 30 DW volumes). From the DvNav sequence we obtain for each volume a measurement of any change in the scanner frequency. To evaluate the spatial shift in the images due to drift in the central frequency throughout each scan, and between successive scans, we co-registered for each scan the first of the navigator pair for each volume to the first navigator image of the first volume of the first scan (scan 1) using AFNI-3dAllineate (Cox, 1996). Better co-registration was achieved using the navigator images instead of the DTI volume images due to DTI contrast changes that occur from volume to volume, which affects the registration process. In this way, we obtained for each volume of each scan a measure of the translation along the phase encode direction resulting from frequency drift.

(2) Comparison between the 3D-EPI phase map of the DvNav sequence and the standard 3D gradient echo phase map—We next compared the performance of the 3D EPI field maps generated by the DvNav to the routinely used 3D gradient echo field maps by examining differences in the b_0 volumes of each. This was done first in a water phantom and then in two volunteers in the absence of explicit motion (each subject was instructed to remain relaxed and still). Human subjects were each scanned with the standard and DvNav sequences, as well as with a T1w anatomical scan. For each subject the relative distortion between successive b_0's was quantified using the affine warping parameters (three each for translation, rotation, scaling and shearing), which were calculated using AFNI-3dAllineate. Using FSL (Smith et al., 2004), the T1w image was tissue segmented with FAST to create WM masks, and linearly registered to b_0 maps with FLIRT, which was implemented with 12 degrees of freedom (DOF) and a mutual information cost function. After mapping to the diffusion space, T1w WM outlines were overlayed on each b_0 volume for a comparison of distortions relative to anatomical images.

(3) Effects of subject motion on DTI data for DvNav, vNav and standard sequences—Finally, we assessed the benefits of real-time simultaneous motion and shim correction on DTI data acquired in the presence of significant subject motion. Two subjects each received three DTI acquisitions: (i) standard without explicit motion; (ii) motion navigated DTI (vNav; implemented using the DvNav sequence with the shim correction

disabled) with motion; and (iii) motion an shim navigated DTI (DvNav) with motion. Before the scan session, participants were instructed that they must move their head when prompted and that they would be prompted to move 5 times during each scan with motion. To ensure that participants moved by approximately the same amount and in a repeatable way, a parallelogram-shaped grid was mounted on the head coil, which subjects could use as a guide during head movements. Subjects practiced moving their head in a repeatable way before the start of the scan.

Identical processing streams were implemented for each of these acquisitions. Retrospective motion correction was implemented with FSL-FLIRT (12 DOF and mutual information cost function). Diffusion tensors (DTs) and associated parameters such as fractional anisotropy (FA) were calculated using FSL. T1w images were segmented and registered to DTI space using FSL.

Results

(1) Validation of DvNav frequency and linear gradient measurements

The errors of the DvNav frequency and linear shim gradient estimates in a water phantom are summarized in Table 1. The results demonstrate that the DvNav sequence accurately estimates these changes over this range of frequency and shim adjustments.

The top row of Figure 3 shows how the images are shifted due to manual adjustments of the scanner frequency, while the bottom row shows the ability of the DvNav sequence to correct the frequency and reduce shifts in the images prior to acquisition of the second volume. Notably, the shift increases with greater frequency offsets and are mainly along the phase encode (vertical) direction. Similarly, Figure 4 shows distortions arising from adjustments of the linear shim gradients by 15 μT/m first along the y- (phase encode) direction, then along the x- (readout) and y-directions simultaneously, and finally along the x-, y- and z-directions simultaneously. It is evident from the absence of signal intensity differences in the bottom row of Figure 4 that the DvNav sequence effectively adjusts the linear shim gradients prior to the acquisition of the second volume, essentially eliminating distortions.

The box-and-whisker plots in Figure 5 show how the scanner central frequency varies over the 38 volumes for each of the five successive scans. Notably, the frequency changes by roughly 15 Hz during a scan of about 6 minutes and the frequency drift increases over time. This effect may result in a significant spatial shift in the phase encode direction in the images, as shown in Figure 6 for the 38 volumes of the five consecutive scans. Even before the completion of the first scan, the observed translation (0.5 mm) is already a significant fraction of the DTI voxel size (2 mm).

(2) Comparison between the 3D-EPI phase map of the DvNav sequence and the standard 3D gradient echo phase map

Figure 7 shows the difference in performance in a water phantom between the static shim of the MRI scanner, which is based on a 3D gradient echo field map acquired before the DTI scan commences, and that of the DvNav sequence (the 3D EPI field map acquired throughout the DTI acquisition) by comparing distortions evident in the first uncorrected b_0

volume to those in the latter b_0 volumes (2 to 8) to which shim correction have been applied. Distortion along the phase encoding (vertical) direction in the first uncorrected b_0 volume is clearly visible as signal loss compared to the corrected volumes at the top and bottom edges of the water phantom.

Figure 8 displays the first four b_0 volumes of a volunteer scanned without explicit motion using the standard (top row) and DvNav (bottom row) DTI sequences, respectively. T1w WM boundaries (shown in blue) are overlaid on each of the b_0 volumes. Locations of large mismatch are highlighted with arrows. Several areas of mismatch are apparent in all b_0 volumes acquired using the standard sequence, particularly in superior and inferior regions. Similar distortions are apparent in the first volume of the DvNav scan, which is acquired before any shim correction has been applied. However, subsequent volumes show noteworthy improvement after shim correction by the DvNav sequence. Results for the second subject were similar.

Figure 9 presents quantitative comparisons of the relative distortions between the first four b_0 volumes acquired using the standard and DvNav sequences. The affine warping parameters between all pairs of b_0 volumes are plotted for two subjects. In the DvNav case, the registration of each of the corrected b_0 volumes (b_0(2-4)) to the uncorrected b_0 volume ($b_0$1) quantifies the amount (and type) of distortion correction effected by the DvNav sequence. Additionally, the stability of the correction can be assessed by registering each of the corrected volumes (b_0(2-4)) to each other, which also provides insight into the scale of the distortion correction relative to noise and other scanner effects. For the standard acquisition, there are minimal scaling, shearing and rotation between pairs of b_0 volumes, while the shift increases slightly for later b_0's (possibly due to motion or shim heating). Notably, the DvNav shows significant shearing and rotation between the initial uncorrected $b_0$1 and the corrected b_0 volumes, while the corrected b_0's (b_0(2-4)) appear homogeneous to each other.

(3) Effects of subject motion on DTI data for DvNav, vNav and standard sequences

The first row of Figure 10 shows changes in motion parameters estimated by the navigator using the PACE algorithm for the vNav and DvNav acquisitions of one subject who was instructed to move 5 times during each scan. The vNav in this case was implemented using the DvNav sequence with shim correction disabled. Since the DvNav sequence was used, field maps were generated throughout the acquisition but shim correction was not applied. Motion parameters are similar for the two scans. The second row shows shifts in the central frequency as measured by the DvNav sequence. Although the frequency shifts are qualitatively similar, the magnitudes differ. Since the DvNav acquisition was performed first, heating of the iron shim coils could have occurred, resulting in a large initial frequency offset in the vNav acquisition. We note that translation along the bore of the magnet (*z*-direction) at volume 32 results in a substantial frequency shift.

The bottom row of Figure 10 demonstrates how the linear shim gradients, as estimated by the DvNav sequence, are affected by subject motion. The data for the vNav acquisition demonstrate that motion correction alone is not able to correct changes in B0 that result from motion. In contrast, the DvNav sequence performs shim correction each time a change is

detected. Shim correction commences after the first DTI volume. We note that the DvNav sequence is able to optimise B0 homogeneity compared to the initial static shimming performed by the scanner. Results for the second subject were similar. Interestingly, changes in the shim gradients are largest at volume 8, even though larger motion is observed at other volumes, presumably due to the relatively large rotation around the *x*-axis (i.e., nodding motion) at this volume, which appears to have a large effect on B0 homogeneity.

The effects of subject motion and resulting changes in B0 on DTI data are compared for standard, vNav and DvNav acquisitions in one subject in Figure 11. The standard scan was acquired with no explicit motion, while the vNav and the DvNav scans were acquired with intentional motion. Motion parameters for this subject are shown in figure 10. All data were analysed using identical processing streams. Thresholded FA maps (FA > 0.2) are overlaid on a T1w WM mask. Despite significant subject motion, the FA map of the DvNav acquisition shows less distortion and better alignment with T1w WM, especially in the anterior regions of the brain (Fig. 11c), than both the vNav acquisition, which had similar motion (Fig. 11b), and the standard acquisition with minimal motion (Fig. 11a).

Discussion

B0 distortion is a complex phenomenon that is characterized by spatially and temporally varying underlying magnetic field inhomogeneities. Although inhomogeneities exist, even in the absence of any object, the presence of an object in the scanner is known to induce large deviations in the field. Subject motion and/or heating of the iron shim coils due to eddy currents or mechanical vibrations can lead to significant temporal fluctuations in B0. All of these processes result in distortions and artefacts in the diffusion data. For example, subject motion typically results in the lowering of FA values in WM as has been demonstrated using whole brain maps and average ROI values (Alhamud et al., 2015) and by comparisons with segmented structural images (Taylor et al., 2015). In the present work we were interested in examining the effects of motion and shim correction on geometric distortion in the images.

Although MRI scanners typically estimate the shim parameters before the start of the DTI scan, there are currently no methods that estimate changes in the field during the lengthy DTI acquisition. Typically, only the b_0 volumes are considered for distortion correction, thus neglecting the field variations that may occur throughout the acquisition (Andersson et al., 2003; Holland et al., 2010). A practical limitation of post-processing corrections is that DWI volumes have much less signal than b_0 images, as well as a contrast that changes with each different gradient application, making registration to the anatomical images for generating deformation maps more complicated.

In the current work we have introduced a double volumetric navigator (DvNav) technique to measure and correct both shim parameters and motion after each navigator pair, which is acquired once per TR. This approach performs volume-by-volume corrections and the navigator protocol is independent of the type of data being acquired. As such, it can be applied to high b-value diffusion weighted techniques and to blood oxygenation level dependent (BOLD) functional MRI (fMRI). Additional factors that may affect navigator

quality (distortion and contrast), such as eddy currents, should be considered in these applications.

We first presented results of several water phantom experiments to quantitatively validate the ability of the DvNav sequence to measure, report and correct the zeroth and first order distortions in the B0 field. Secondly, we demonstrated how the shims in the MRI scanner change, both across consecutive DTI scans and within individual acquisitions. This point is important in view of studies that use consecutive DTI scans with either different phase encoding directions (Andersson et al., 2003) or a longer diffusion table, such as in q-space imaging (Assaf and Cohen, 1999), HARDI (Tuch et al., 2002), and diffusion spectrum imaging (Wedeen et al., 2005). Further, we demonstrated how B0 field changes can affect DTI results, both with and without subject motion. We also presented data to illustrate the differences between the static shim prepared by the MRI scanner and the shim correction performed by the DvNav sequence.

The DvNav sequence was shown to accurately measure and correct ΔB0 following manual manipulations of the scanner central frequency and the linear shim gradients. Drift in the system frequency can influence the effectiveness of fat suppression (Benner et al., 2006) or any selective excitation pulses. The manipulation of the linear shim gradients causes geometrical distortions with intensity variations especially when more than one shim term has been adjusted. Thus, it is important for data quality that the shim be corrected as each new volume is acquired. In all scans, differences in images following static shimming by the MRI scanner, which uses a 3D gradient echo field map, compared to dynamic shimming by the 3D EPI map of the DvNav sequence were observed primarily along the phase encoding direction. The effects of these distortions were clearly visible when thresholded FA maps were overlaid on WM masks obtained from segmentation of T1w images. Shearing distortion (particularly inferiorly and superiorly) was more evident in scans acquired using the scanner's standard static shim. Distortions were consistently reduced in the DvNav scans.

Approaches for ΔB0 correction, which include field maps and nonlinear registration, as well as the acquisition of additional EPI images with opposite phase encoding directions, assume that the amount of distortion remains unchanged thoughout the DTI acquisition. We have illustrated that this is not the case in the presence of subject motion, and even in some cases when there is no subject motion. The drift in the system frequency could be very sensitive to the heating of the iron shim coils and the drift may accumulate within a scan and from one scan to the next. In the present study, the total shift along the phase encoding direction after 5 consecutive scans was greater than the DTI acquisition's 2 mm voxel size. Furthermore, subject motion induces shim changes that differ based on the nature of the motion. For example, although the amount of rotation (3°) around the x-axis at volume 32 was less than at volume 8 (5°), the drift in the scanner central frequency due to the former was substantially larger (Figure 10). The difference between the motion at these two volumes is that the former (volume 32) was accompanied by a large translation along the bore of the magnet, evident in both the vNav and the DvNav acquisitions. It appears from these results that translation along the bore of the magnet significantly affects the scanner central frequency. Additionally, nodding motion (i.e., rotation around the x-axis) has the largest

effect on the linear shim gradients, especially the y component, as can be seen at volumes 8, 14 and 32. These observations are in agreement with those of others (Hess et al., 2011; Keating and Ernst, 2012). In this study, it has been demonstrated that prospective motion correction alone does not correct B0 changes resulting from this motion.

Using the second navigator in the DvNav sequence, shim changes from various sources can be corrected prior to each volume acquisition. This was particularly apparent in the volunteer scans where FA maps acquired with significant subject motion and DvNav correction showed reduced image distortion in the anterior region of the brain compared even to the scan acquired with minimal motion using the standard sequence.

Current limitations and further developments for the DvNav Sequence

Since the current DvNav sequence only applies position and shim correction to the following DTI volume, it cannot correct changes in position or shim that occur continuously throughout the scan. Motion may also occur during or between the acquisition of the two navigators, or following the navigators. The DvNav sequence is designed to evaluate shim and motion independently of the previous pair of navigators. The time between acquisition of the navigator and application of the position and shim corrections is approximately 1.1 s. To speed up motion and shim corrections, a DvNav could be inserted after every N slices (e.g., once every 5 slices). In this manner, total acquisition time can be traded for more frequent corrections and correspondingly higher quality data.

Although in this work we have only evaluated ΔB0 in terms of zeroth and first order shims, in principle the DvNav sequence is also able to measure second or higher order shims from the 3D EPI field map. These terms are fitted to the data using the same algorithm. However, with the current hardware 2^{nd} or higher order shims cannot be updated in real time. Correcting for higher order shims may be severely limited by eddy currents and resulting eddy fields produced by the switching of high order unshielded shim gradient coils. In contrast, eddy current effects produced by first order gradient switching is usually minimized by shielded gradient designs.

In the current design of the DvNav sequence, the additional time for acquisition of the two navigators, as well as the computational processes, is around 1150 ms (2×475 ms for the navigator acquisition, 80 ms for the motion correction calculation, and 120 ms for the shim correction calculation) for each TR. This equates to roughly an additional 44s for 30 diffusion directions and 8 b_0 volumes. This time could be decreased by using a lower navigator resolution such as 32×32×16 mm^3, parallel or simultaneous multislice imaging (Bhat et al., 2014), radial or spiral trajectories instead of a Cartesian trajectory, and faster algorithms or computers for motion correction.

Although the number of b_0s in the current protocol was 8, this number can be reduced. In the current design of the DvNav sequence, the shim correction starts immediately after the first b_0 volume. However, for more accurate shim correction, we recommend using at least three b_0's, since the stability in the shim adjustment increases after volume 2. Since motion could occur at volumes 1 or 2, which would distort the corrected b_0 volumes, the number of b_0's used is a trade-off between total scan time and a good shim correction.

In the current design of the DvNav sequence, we calculate separate field maps for DTI and the navigator since their FOVs differ. A new function will be added to calculate only one field map in cases when the FOVs are identical. This will reduce the scan time by 50 ms.

While the results presented in this paper are for shim correction over the whole FOV of the DTI acquisition, the DvNav sequence is being adapted to measure and adjust shim over selected regions of the DTI 'slab-by-slab'. Parallel imaging is another field that could benefit significantly from this technique, since the difference in sensitivities between individual coil elements in a receive array may be affected by motion as well as distortions in the B0 field.

Conclusions

It is well known that variations in the B0 field can lead to geometrical distortions and signal intensity variations. The magnitude of these effects can become particularly severe in the presence of subject motion. The drift in the system central frequency differs across scans as well as within individual acquisitions, likely often due to the heating of the shim iron. This decreases the stability of the acquisition. We have proposed a double navigator (DvNav) technique that can accurately measure changes in the static B0 field under a wide range of conditions. Moreover, this double navigator method enables simultaneous correction for both subject motion and B0 distortion following the acquisition of each DTI measurement. The proposed method overcomes most of the limitations of current methods for B0 correction in DTI in that ΔB0 can be evaluated and corrected at each point of the DTI series. The generality of the double navigator approach may also be directly extended to other imaging modalities, such fMRI and high field MRI.

References

Aksoy M, Forman C, Straka M, Skare S, Holdsworth S, Hornegger J, Bammer R. Real-time optical motion correction for diffusion tensor imaging. Magnetic resonance in medicine. 2011; 66:366–378. [PubMed: 21432898]

Alhamud, A.; Hess, AT.; Tisdall, MD.; Meintjes, EM.; van der Kouwe, AJ. Implementation of real time motion correction in diffusion tensor imaging. Proceedings of the 19th Annual Meeting of ISMRM; May; Montreal, Canada. 2011.

Alhamud A, Taylor PA, Laughton B, van der Kouwe AJ, Meintjes EM. Motion artifact reduction in pediatric diffusion tensor imaging using fast prospective correction. Journal of magnetic resonance imaging. 2015; 41:1353–1364. [PubMed: 24935904]

Alhamud A, Tisdall MD, Hess AT, Hasan KM, Meintjes EM, van der Kouwe AJ. Volumetric navigators for real-time motion correction in diffusion tensor imaging. Magnetic resonance in medicine. 2012; 68:1097–1108. [PubMed: 22246720]

Andersson JL, Skare S, Ashburner J. How to correct susceptibility distortions in spin-echo echo-planar images: application to diffusion tensor imaging. Neuroimage. 2003; 20:870–888. [PubMed: 14568458]

Assaf Y, Cohen Y. Structural information in neuronal tissue as revealed by q-space diffusion NMR spectroscopy of metabolites in bovine optic nerve. NMR in Biomedicine. 1999; 12:335–344. [PubMed: 10516615]

Bammer R, Auer M, Keeling SL, Augustin M, Stables LA, Prokesch RW, Stollberger R, Moseley ME, Fazekas F. Diffusion tensor imaging using single-shot SENSE-EPI. Magnetic resonance in medicine. 2002; 48:128–136. [PubMed: 12111940]

Basser PJ, Mattiello J, LeBihan D. MR diffusion tensor spectroscopy and imaging. Biophysical journal. 1994; 66:259. [PubMed: 8130344]

Behrens T, Johansen-Berg H, Woolrich M, Smith S, Wheeler-Kingshott C, Boulby P, Barker G, Sillery E, Sheehan K, Ciccarelli O. Non-invasive mapping of connections between human thalamus and cortex using diffusion imaging. Nature neuroscience. 2003; 6:750–757. [PubMed: 12808459]

Benner T, van der Kouwe AJ, Kirsch JE, Sorensen AG. Real-time RF pulse adjustment for B0 drift correction. Magnetic resonance in medicine. 2006; 56:204–209. [PubMed: 16767763]

Benner T, van der Kouwe AJ, Sorensen AG. Diffusion imaging with prospective motion correction and reacquisition. Magnetic resonance in medicine. 2011; 66:154–167. [PubMed: 21695721]

Bennett IJ, Rypma B. Advances in functional neuroanatomy: A review of combined DTI and fMRI studies in healthy younger and older adults. Neuroscience & Biobehavioral Reviews. 2013; 37:1201–1210. [PubMed: 23628742]

Bhat, H.; Cauley, S.; Tisdall, MD.; Witzel, T.; Setsompop, K.; van der Kouwe, AJW.; Heberlein, K. Prospective motion correction based on ultra-fast whole head navigators acquired with Multi-Band EPI. ISMRM Workshop on Motion Correction in MRI; July; Tromsø, Norway. 2014.

Bhat, H.; Tisdall, MD.; van der Kouwe, AJW.; Feiweier, T.; Heberlein, K. EPI navigator based prospective motion correction technique for diffusion neuroimaging. Proceedings of the 19th Annual Meeting of ISMRM; May; Melbourne, Australia. 2012.

Buonocore MH, Gao L. Ghost artifact reduction for echo planar imaging using image phase correction. Magnetic resonance in medicine. 1997; 38:89–100. [PubMed: 9211384]

Cox RW. AFNI: software for analysis and visualization of functional magnetic resonance neuroimages. Computers and Biomedical research. 1996; 29:162–173. [PubMed: 8812068]

El-Sharkawy AM, Schär M, Bottomley PA, Atalar E. Monitoring and correcting spatio-temporal variations of the MR scanner's static magnetic field. Magnetic Resonance Materials in Physics, Biology and Medicine. 2006; 19:223–236.

Engelbrecht V, Scherer A, Rassek M, Witsack HJ, Modder U. Diffusion-weighted MR imaging in the brain in children: findings in the normal brain and in the brain with white matter diseases 1. Radiology. 2002; 222:410–418. [PubMed: 11818607]

Foerster BU, Tomasi D, Caparelli EC. Magnetic field shift due to mechanical vibration in functional magnetic resonance imaging. Magnetic resonance in medicine. 2005; 54:1261–1267. [PubMed: 16215962]

Hasan KM, Walimuni IS, Abid H, Frye RE, Ewing-Cobbs L, Wolinsky JS, Narayana PA. Multimodal quantitative magnetic resonance imaging of thalamic development and aging across the human lifespan: implications to neurodegeneration in multiple sclerosis. The Journal of Neuroscience. 2011; 31:16826–16832. [PubMed: 22090508]

Hess AT, Dylan Tisdall M, Andronesi OC, Meintjes EM, van der Kouwe AJ. Real-time motion and B0 corrected single voxel spectroscopy using volumetric navigators. Magnetic resonance in medicine. 2011; 66:314–323. [PubMed: 21381101]

Holland D, Kuperman JM, Dale AM. Efficient correction of inhomogeneous static magnetic field-induced distortion in Echo Planar Imaging. Neuroimage. 2010; 50:175–183. [PubMed: 19944768]

Huang H, Ceritoglu C, Li X, Qiu A, Miller MI, van Zijl PC, Mori S. Correction of B0 susceptibility induced distortion in diffusion-weighted images using large-deformation diffeomorphic metric mapping. Magnetic resonance imaging. 2008; 26:1294–1302. [PubMed: 18499384]

Irfanoglu MO, Walker L, Sarlls J, Marenco S, Pierpaoli C. Effects of image distortions originating from susceptibility variations and concomitant fields on diffusion MRI tractography results. Neuroimage. 2012; 61:275–288. [PubMed: 22401760]

Itahashi T, Yamada T, Nakamura M, Watanabe H, Yamagata B, Jimbo D, Shioda S, Kuroda M, Toriizuka K, Kato N. Linked alterations in gray and white matter morphology in adults with high-functioning autism spectrum disorder: A multimodal brain imaging study. NeuroImage: Clinical. 2015; 7:155–169. [PubMed: 25610777]

Jenkinson M. Fast, automated, N-dimensional phase-unwrapping algorithm. Magnetic resonance in medicine. 2003; 49:193–197. [PubMed: 12509838]

Jezzard P, Balaban RS. Correction for geometric distortion in echo planar images from B0 field variations. Magnetic resonance in medicine. 1995; 34:65–73. [PubMed: 7674900]

Keating B, Ernst T. Real-time dynamic frequency and shim correction for single-voxel magnetic resonance spectroscopy. Magnetic resonance in medicine. 2012; 68:1339–1345. [PubMed: 22851160]

Kober T, Gruetter R, Krueger G. Prospective and retrospective motion correction in diffusion magnetic resonance imaging of the human brain. Neuroimage. 2012; 59:389–398. [PubMed: 21763773]

Kybic J, Thévenaz P, Nirkko A, Unser M. Unwarping of unidirectionally distorted EPI images. Medical Imaging, IEEE Transactions on. 2000; 19:80–93.

Le Bihan D, Poupon C, Amadon A, Lethimonnier F. Artifacts and pitfalls in diffusion MRI. Journal of magnetic resonance imaging. 2006; 24:478–488. [PubMed: 16897692]

Lee SK, Tan ET, Govenkar A, Hancu I. Dynamic slice-dependent shim and center frequency update in 3 T breast diffusion weighted imaging. Magnetic resonance in medicine. 2014; 71:1813–1818. [PubMed: 23798360]

Miller JH, McKinstry RC, Philip JV, Mukherjee P, Neil JJ. Diffusion-tensor MR imaging of normal brain maturation: a guide to structural development and myelination. American Journal of Roentgenology. 2003; 180:851–859. [PubMed: 12591710]

Morrell G, Spielman D. Dynamic shimming for multi-slice magnetic resonance imaging. Magnetic resonance in medicine. 1997; 38:477–483. [PubMed: 9339449]

Mukherjee P, Miller JH, Shimony JS, Conturo TE, Lee BC, Almli CR, McKinstry RC. Normal Brain Maturation during Childhood: Developmental Trends Characterized with Diffusion-Tensor MR Imaging. Radiology. 2001; 221:349–358. [PubMed: 11687675]

Noriuchi M, Kikuchi Y, Yoshiura T, Kira R, Shigeto H, Hara T, Tobimatsu S, Kamio Y. Altered white matter fractional anisotropy and social impairment in children with autism spectrum disorder. Brain research. 2010; 1362:141–149. [PubMed: 20858472]

Pavuluri MN, Yang S, Kamineni K, Passarotti AM, Srinivasan G, Harral EM, Sweeney JA, Zhou XJ. Diffusion tensor imaging study of white matter fiber tracts in pediatric bipolar disorder and attention-deficit/hyperactivity disorder. Biological psychiatry. 2009; 65:586–593. [PubMed: 19027102]

Pfeuffer J, de Moortele V, Ugurbil K, Hu X, Glover GH. Correction of physiologically induced global off-resonance effects in dynamic echo-planar and spiral functional imaging. Magnetic resonance in medicine. 2002; 47:344–353. [PubMed: 11810679]

Pierpaoli C, Walker L, Irfanoglu M, Barnett A, Basser P, Chang L, Koay C, Pajevic S, Rohde G, Sarlls J. TORTOISE: an integrated software package for processing of diffusion MRI data. Book TORTOISE: an integrated software package for processing of diffusion MRI data. 2010; 18:1597. Editor ed^ eds.

Pruessmann KP, Weiger M, Scheidegger MB, Boesiger P. SENSE: sensitivity encoding for fast MRI. Magnetic resonance in medicine. 1999; 42:952–962. [PubMed: 10542355]

Qiu D, Tan LH, Zhou K, Khong PL. Diffusion tensor imaging of normal white matter maturation from late childhood to young adulthood: voxel-wise evaluation of mean diffusivity, fractional anisotropy, radial and axial diffusivities, and correlation with reading development. Neuroimage. 2008; 41:223–232. [PubMed: 18395471]

Reese T, Heid O, Weisskoff R, Wedeen V. Reduction of eddy-current-induced distortion in diffusion MRI using a twice-refocused spin echo. Magnetic resonance in medicine. 2003; 49:177–182. [PubMed: 12509835]

Rohde G, Barnett A, Basser P, Marenco S, Pierpaoli C. Comprehensive approach for correction of motion and distortion in diffusion-weighted MRI. Magnetic resonance in medicine. 2004; 51:103–114. [PubMed: 14705050]

Ruthotto L, Kugel H, Olesch J, Fischer B, Modersitzki J, Burger M, Wolters C. Diffeomorphic susceptibility artifact correction of diffusion-weighted magnetic resonance images. Physics in medicine and biology. 2012; 57:5715. [PubMed: 22941943]

Schmithorst VJ, Wilke M, Dardzinski BJ, Holland SK. Correlation of White Matter Diffusivity and Anisotropy with Age during Childhood and Adolescence: A Cross-sectional Diffusion-Tensor MR Imaging Study. Radiology. 2002; 222:212–218. [PubMed: 11756728]

Smith SM, Jenkinson M, Woolrich MW, Beckmann CF, Behrens TE, Johansen-Berg H, Bannister PR, De Luca M, Drobnjak I, Flitney DE. Advances in functional and structural MR image analysis and implementation as FSL. Neuroimage. 2004; 23:S208–S219. [PubMed: 15501092]

Snook L, Paulson LA, Roy D, Phillips L, Beaulieu C. Diffusion tensor imaging of neurodevelopment in children and young adults. Neuroimage. 2005; 26:1164–1173. [PubMed: 15961051]

Staempfli P, Reischauer C, Jaermann T, Valavanis A, Kollias S, Boesiger P. Combining fMRI and DTI: a framework for exploring the limits of fMRI-guided DTI fiber tracking and for verifying DTI-based fiber tractography results. Neuroimage. 2008; 39:119–126. [PubMed: 17931889]

Studholme C, Constable RT, Duncan JS. Accurate alignment of functional EPI data to anatomical MRI using a physics-based distortion model. Medical Imaging, IEEE Transactions on. 2000; 19:1115–1127.

Tao, R.; Fletcher, PT.; Gerber, S.; Whitaker, RT. Information Processing in Medical Imaging. Springer; 2009. A variational image-based approach to the correction of susceptibility artifacts in the alignment of diffusion weighted and structural MRI; p. 664-675.

Taylor, PA.; Alhamud, A.; van der Kouwe, AJ.; Saleh, MG.; Laughton, B.; Meintjes, EM. A comparison of combined acquisition and processing methods for DTI: a pediatric study. OHBM; June; Hawaii, USA. 2015.

Thesen S, Heid O, Mueller E, Schad LR. Prospective acquisition correction for head motion with image-based tracking for real-time fMRI. Magnetic resonance in medicine. 2000; 44:457–465. [PubMed: 10975899]

Tisdall MD, Hess AT, Reuter M, Meintjes EM, Fischl B, van der Kouwe AJ. Volumetric navigators for prospective motion correction and selective reacquisition in neuroanatomical MRI. Magnetic resonance in medicine. 2012; 68:389–399. [PubMed: 22213578]

Tuch DS, Reese TG, Wiegell MR, Makris N, Belliveau JW, Wedeen VJ. High angular resolution diffusion imaging reveals intravoxel white matter fiber heterogeneity. Magnetic resonance in medicine. 2002; 48:577–582. [PubMed: 12353272]

van der Kouwe AJ, Benner T, Salat DH, Fischl B. Brain morphometry with multiecho MPRAGE. Neuroimage. 2008; 40:559–569. [PubMed: 18242102]

Ward HA, Riederer SJ, Jack CR. Real-time autoshimming for echo planar timecourse imaging. Magnetic resonance in medicine. 2002; 48:771–780. [PubMed: 12417991]

Wedeen VJ, Hagmann P, Tseng WYI, Reese TG, Weisskoff RM. Mapping complex tissue architecture with diffusion spectrum magnetic resonance imaging. Magnetic resonance in medicine. 2005; 54:1377–1386. [PubMed: 16247738]

Wu, M.; Chang, L-C.; Walker, L.; Lemaitre, H.; Barnett, AS.; Marenco, S.; Pierpaoli, C. Medical Image Computing and Computer-Assisted Intervention–MICCAI 2008. Springer; 2008. Comparison of EPI distortion correction methods in diffusion tensor MRI using a novel framework; p. 321-329.

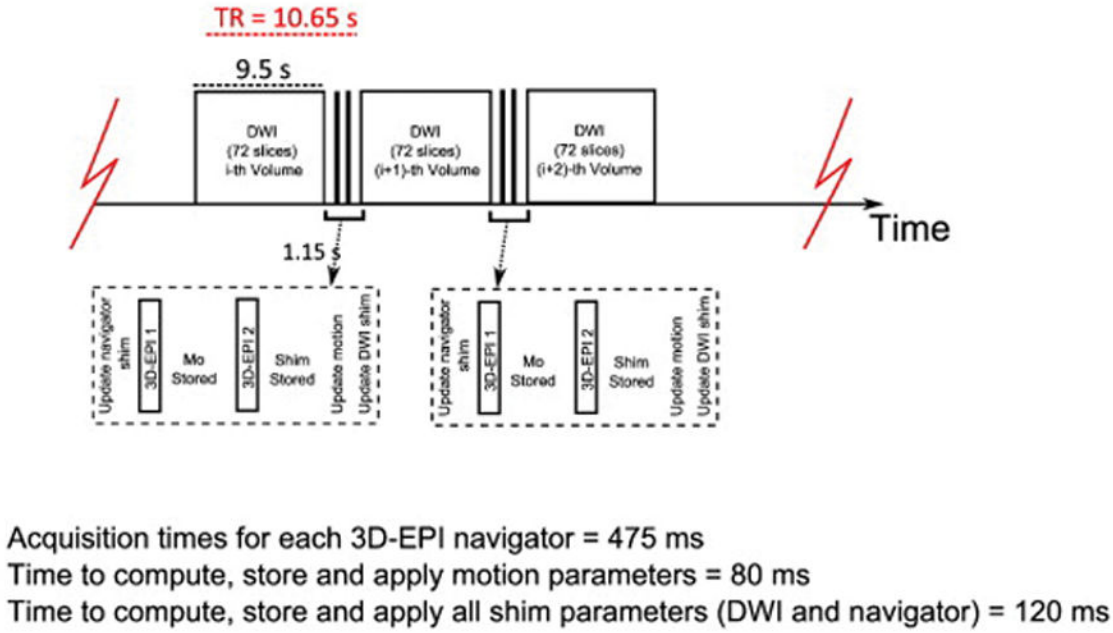

Fig. 1.

Sequence timing diagram of the standard twice-refocused, 2D diffusion pulse sequence (Reese et al., 2003) with double volumetric navigators inserted for simultaneous motion and shim correction.

Acquisition times for ea ch 3D-EPI navigator = 475 ms

Time to com pute, store and ap ply motion parameters = 80 ms

Time to com pute, store and ap ply all shim parameters (DWI and navigator) = 120 ms

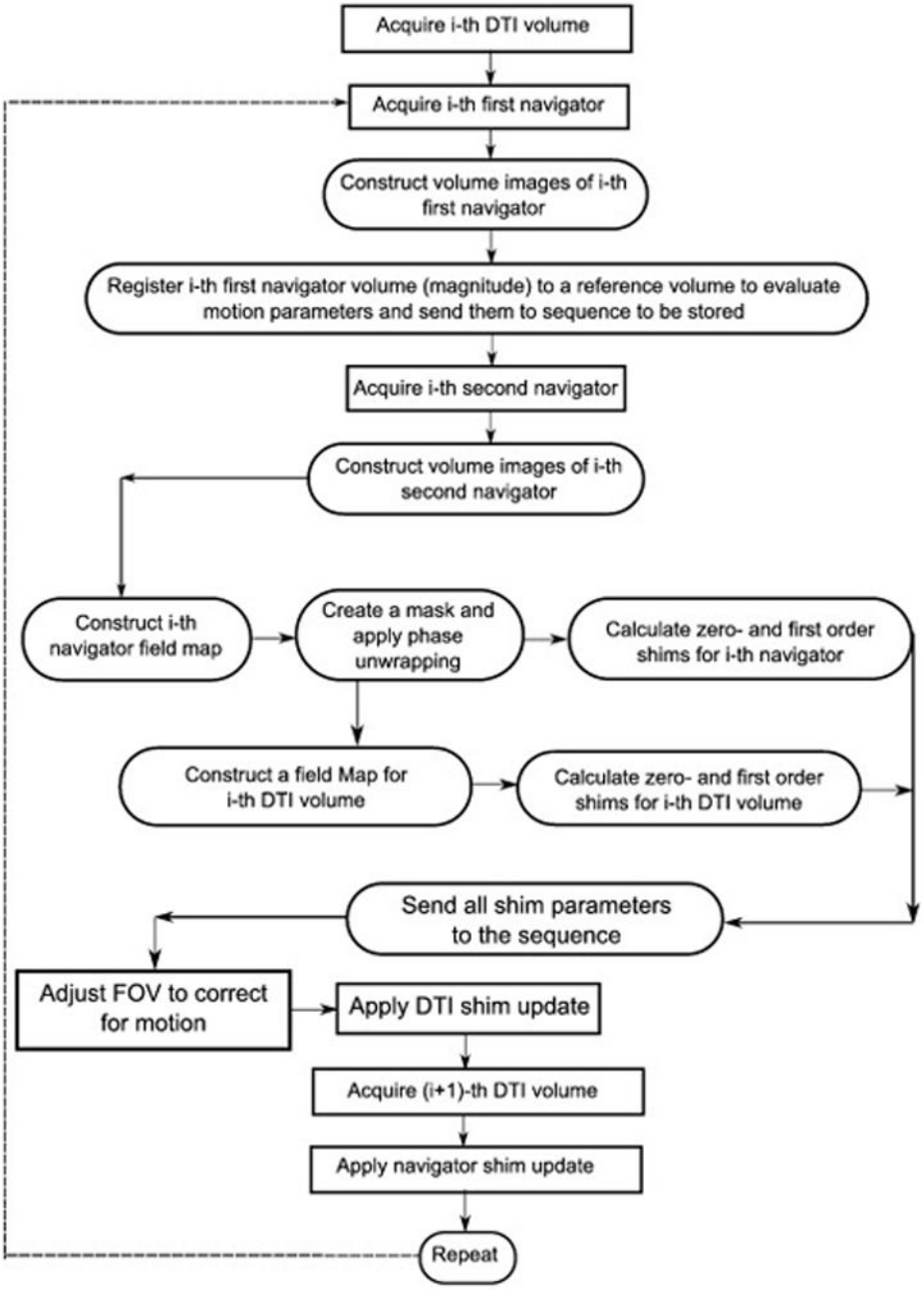

Fig. 2.

A flowchart showing the different steps performed to achieve real time motion and shim correction in the DvNav sequence. Events in rectangular boxes are performed in the sequence acquisition environment, while steps in the rounded rectangular boxes are performed in the image reconstruction environment.

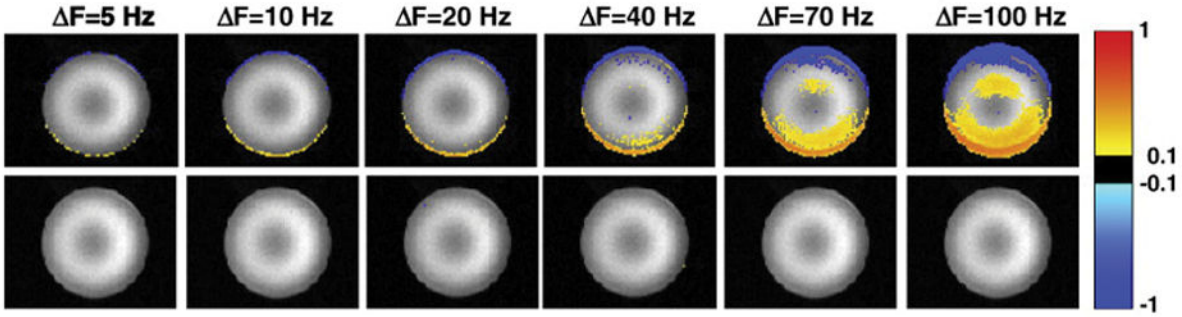

Fig. 3.

Differences in normalized signal intensity between an undistorted reference scan (with zero frequency offset) and scans in which the system central frequency had been adjusted manually by ΔF=5, 10, 20, 40, 70 and 100 Hz, respectively. The top row shows, in a representative slice, the difference between the first volume of each distorted scan and the second volume of the reference scan. The bottom row shows the difference between the second volume of each distorted scan (after which frequency correction has been applied by the DvNav sequence) and the second volume of the reference scan (readout = left to right; phase encode = vertically upwards).

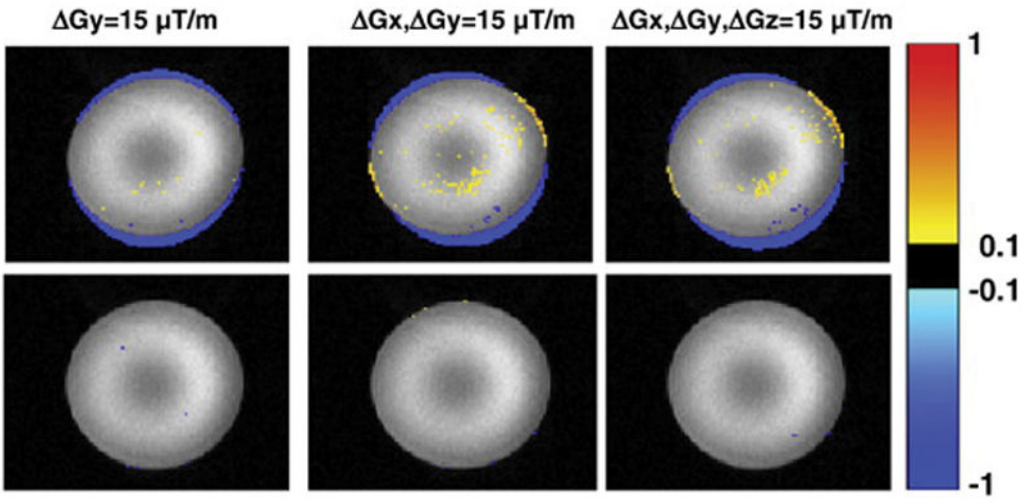

Fig. 4.

Differences in normalized signal intensity between a reference scan and scans in which the linear shim gradients had been adjusted manually (15 μT/m in each stated direction). The top row shows, in a representative slice, the difference between the first volume of the distorted acqusitions and the second volume of the reference scan. The bottom row shows the difference between the second volume of the distorted acquisitions (for which real-time shim correction had been applied) and the second volume of the reference scan. (readout = left to right; phase encode = vertically upwards).

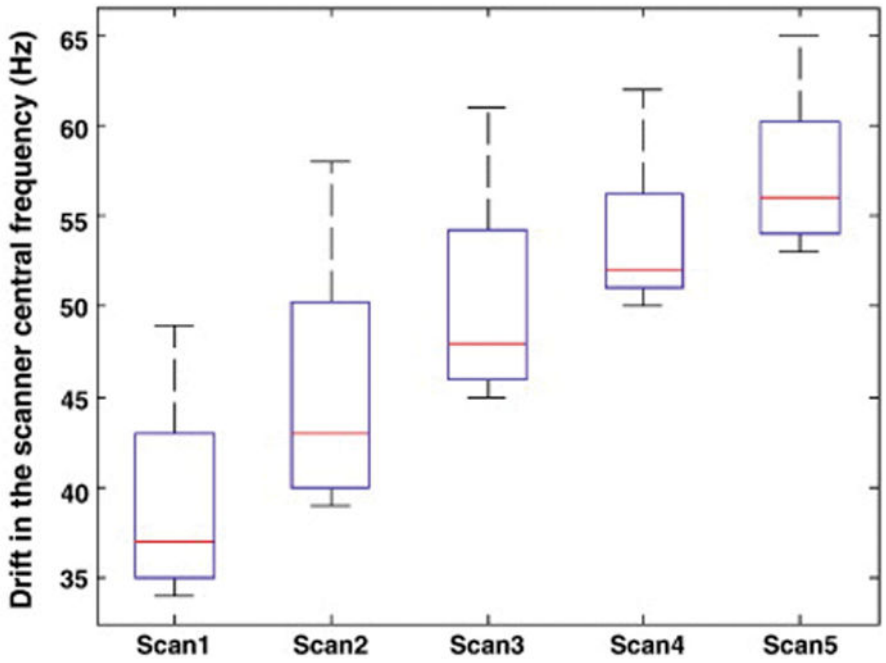

Fig. 5.

Box-and-whisker plots showing the changes in the scanner central frequency estimated by the DvNav sequence for the 38 volumes of 5 consecutive DTI scans. The acquisition time for each scan was 6.7 mins. After the acquisition of the 5 scans (~ 33 mins), the water resonance frequency had drifted by roughly 30 Hz.

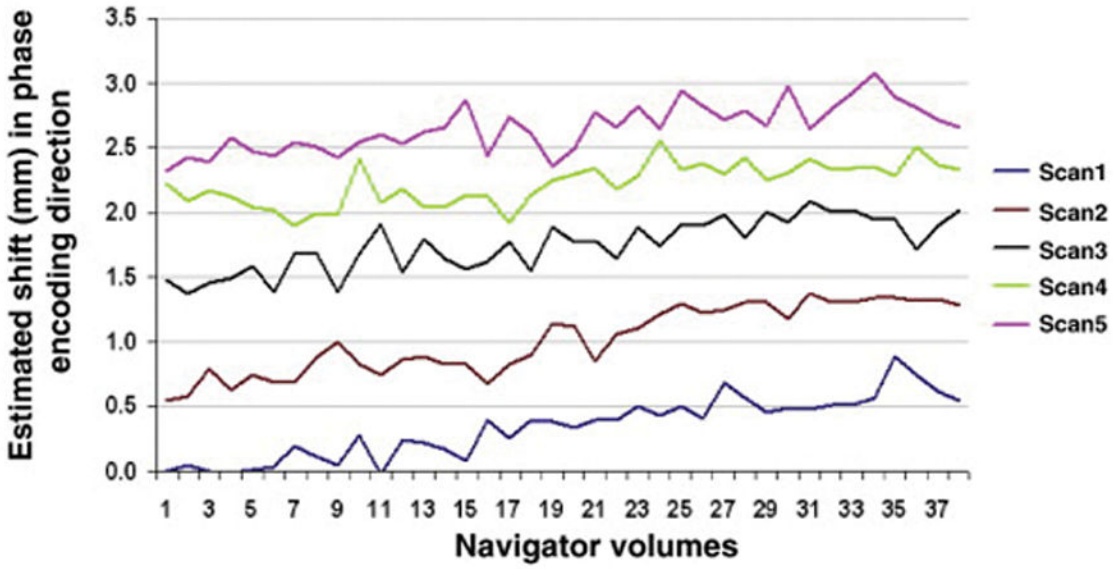

Fig. 6.

Translation (in mm) along the phase encode direction for each navigator volume for each successive scan. The shifts were estimated by registering successive navigators to the first navigator volume of the first scan.

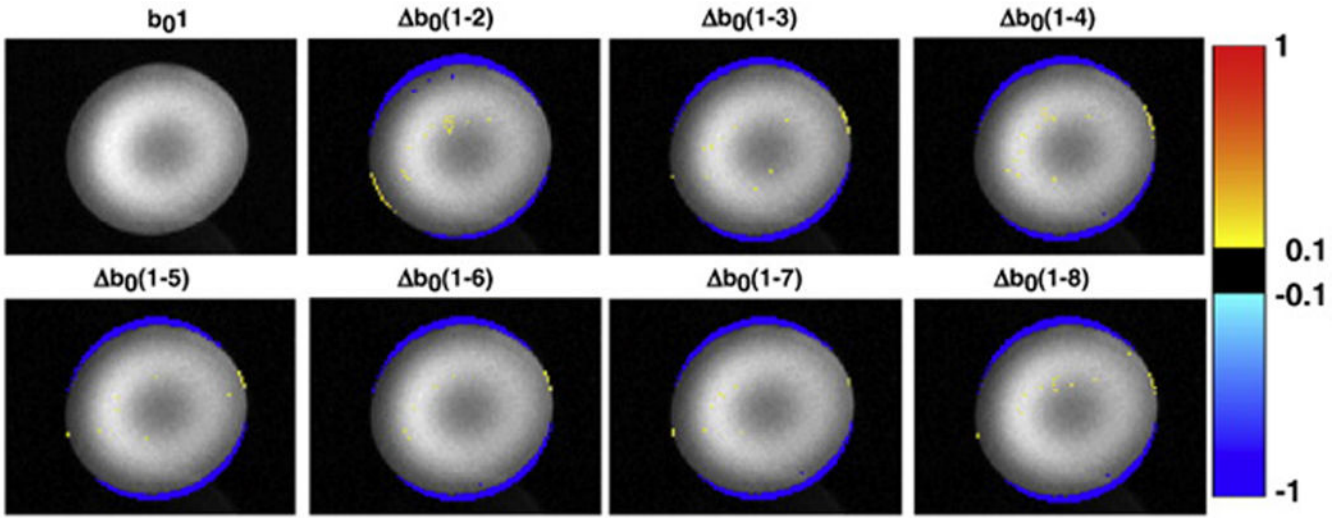

Fig. 7.

Differences in normalized signal intensity between the first b_0 volume (corrected only by the static shim of the MRI scanner) and the next seven b_0 volumes (corrected by DvNav). For example, $\Delta b_0(1\text{-}2) = b_01 – b_02$. (readout = left to right; phase encode = vertically upwards).

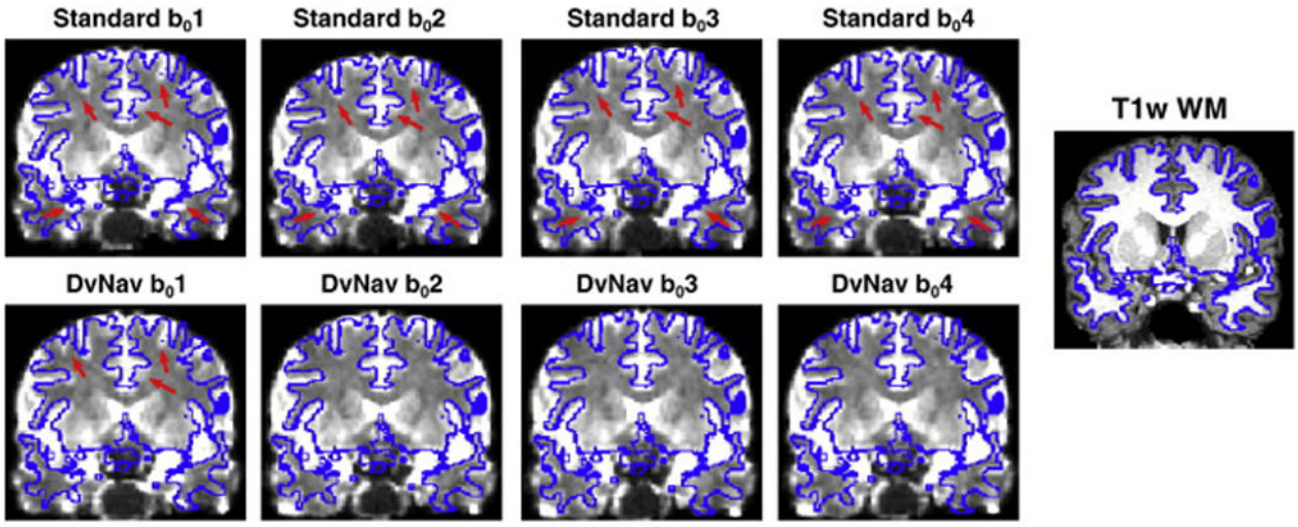

Fig. 8.

A comparison of spatial distortions arising from standard and DvNav acquisitions. The outline of the T1w WM mask is overlaid in blue on each of the first four b_0 volumes from the standard (top row) and DvNav (bottom row) acquisitions. Arrows highlight areas of significant distortion. (readout = left to right; phase encode = anterior to posterior).

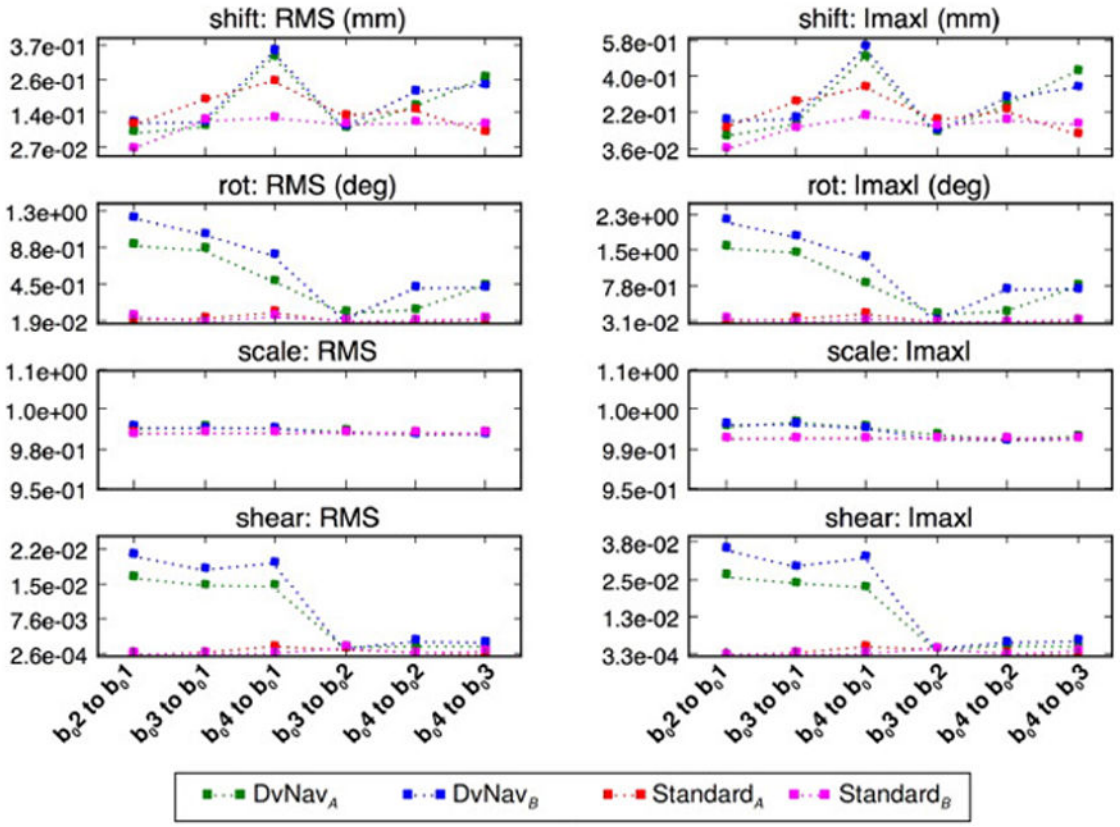

Fig. 9.

A comparison of the magnitudes of the different affine transformation parameters for pairwise registration of the first four b_0 volumes acquired using the standard (hot colors) and DvNav (cool colors) sequences in two subjects (A and B). In the DvNav acquisition correction is applied after the first volume. As such, registration of the corrected b_0 volumes (b_0(2-4)) to the uncorrected $b_0$1 volume quantifies the amount (and type) of distortion correction effected by the DvNav sequence.

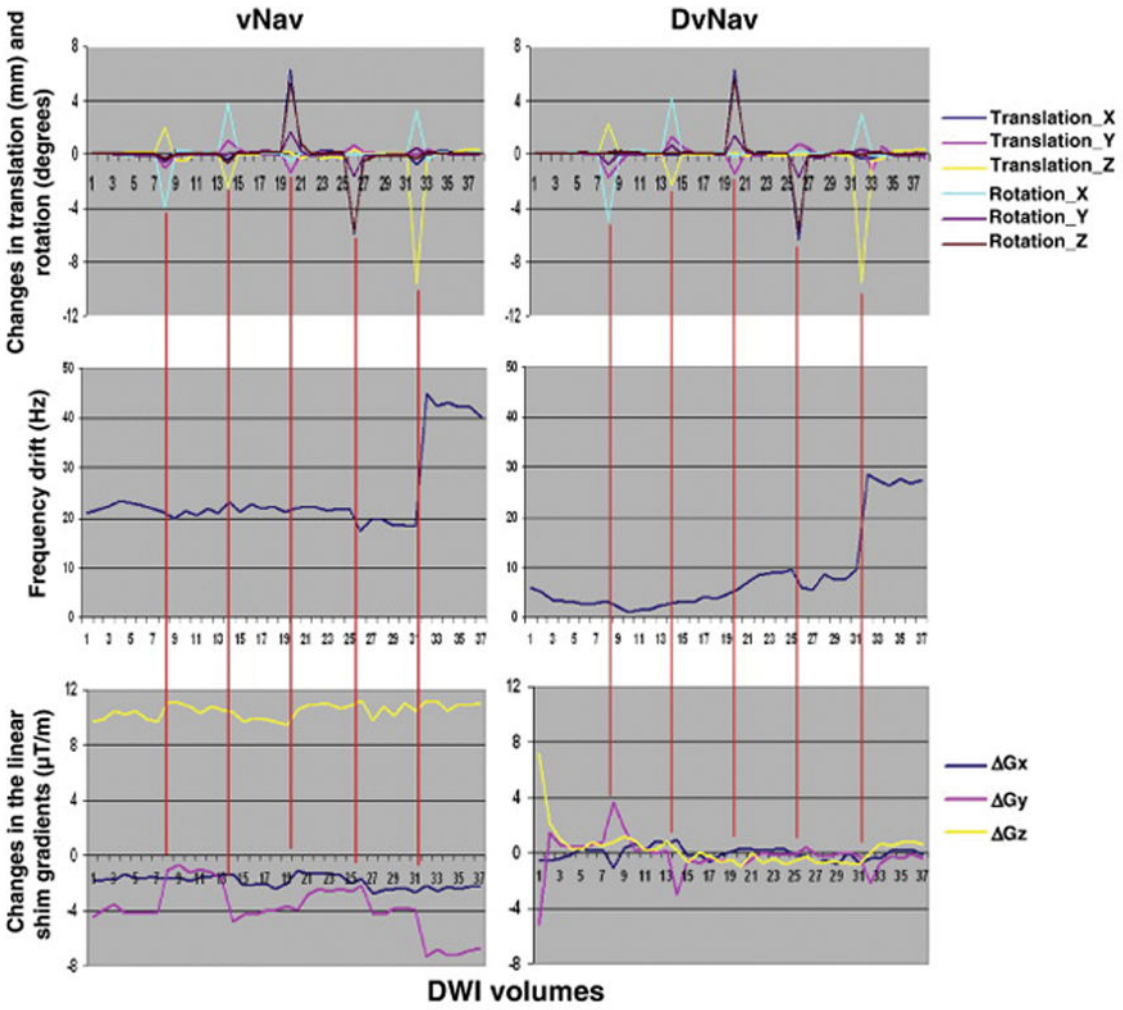

Fig. 10.

Comparison of motion derivatives (1st row), zero (2nd row) and first order shim (3rd row) parameters for a scan with only prospective motion correction (left) and a scan with both real-time motion and shim correction (right).

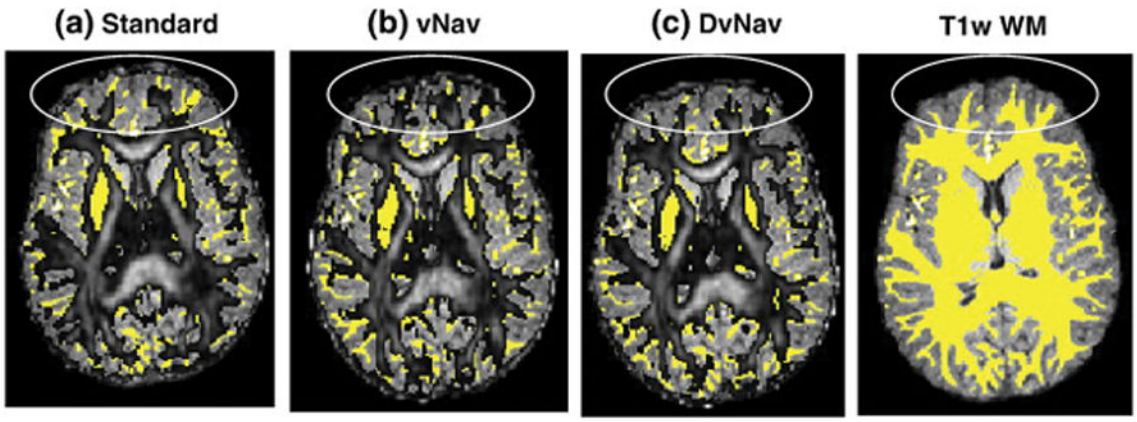

Fig. 11.

FA maps (0.2<FA<1) from (a) standard, (b) vNav (motion correction only), and (c) DvNav acquisitions overlaid on T1w WM masks (yellow). The ovals show regions of high distortion. (readout = left to right; phase encode = anterior to posterior).

Table 1

Errors in the (a) frequency and (b) linear shim gradient changes estimated by the DvNav sequence for different manually applied frequency and gradient shifts. The small increasing positive offset in the frequency estimates may be due to accumulated heating of the shim iron throughout the repeated acquisitions.

(a) Frequency Shifts		**(b) Linear shim gradient Changes**	
Applied Frequency shift (Hz)	**Error in Frequency shift estimated by DvNav (Hz)**	**Applied Linear shim gradient changes (μT/m)**	**Error in Linear shim gradient changes estimated by DvNav (μT/m)**
5.0	−0.1	$G_y = 15.0$	$G_y = 0.2$
10.0	1.2		
20.0	1.4	$G_x = 15.0, G_y = 15.0$	$G_x = 0.0, G_y = 0.4$
40.0	1.9		
70.0	3.5	$G_x = 15.0, G_y = 15.0, G_z = 15.0$	$G_x = -0.2, G_y = 1.0, G_z = -0.1$
100.0	5.1		
Mean Error (RMSE)	2.2 (2.7)	Mean Error (RMSE)	0.2 (0.5)